Supporting Information

Grocholski et al. 10.1073/pnas.1109204109

Materials and Methods.

For pyrolitic and midocean ridge basaltic (MORB) compositions, glass starting materials were synthesized with the levitation method (1) in a reducing atmosphere buffered by a CO/CO_2 gas mixture. We used renormalized oxide ratios of SiO_2, Al_2O_3, FeO, and MgO for the pyrolitic composition from McDonough and Sun (2). The expected amount of Al_2O_3 in Mg-silicate (perovskite, Pv, or postperovskite, pPv) for our pyrolitic sample remains the same as that expected for the pyrolitic composition in McDonough and Sun (2) (5–6 wt% Al_2O_3). We do not include CaO in our pyrolitic starting material to avoid the diffraction peaks of Ca-silicate perovskite (Ca-Pv). Ca-Pv comprises only 5 mol% of the phase assemblage in pyrolite, remains pure (3), and therefore does not influence the depth and thickness of the Pv → pPv transition through element partitioning.

To maximize our ability to determine the effect of ferropericlase (Fp) and Al on the system, we use a natural San Carlos olivine, $(Mg_{0.89}Fe_{0.11})_2SiO_4$. San Carlos olivine contains no Al, whereas pyrolite does. San Carlos olivine composition produces 50 mol% Fp at lower-mantle pressures, whereas pyrolite produces approximately 30 mol% Fp.

For the MORB composition, we took the ratios among SiO_2, Al_2O_3, FeO, MgO, CaO, and Na_2O of normal MORB (4). For the synthesis of MORB glass, we used a mixture of synthetic oxides of SiO_2, Al_2O_3, FeO, and MgO, with a $CaSiO_3$ glass previously synthesized by laser levitation, and $NaAlSi_3O_8$, a natural Amelia albite (Mineralogical Museum at Harvard University, sample #126680). The compositions of the starting materials were determined by electron microprobe analysis at the Massachusetts Institute of Technology and those of pyrolitic and MORB glasses are presented Table S1. Due to some volatile loss during glass synthesis, the oxide ratios of the glass products are slightly different from the original mixtures. However, the difference does not exceed 1%.

Results.

Pyrolitic Composition. Two of the samples from pyrolitic starting material were heated to 2,000–2,500 K at 124 GPa and 1,600–2,600 K at 130 GPa with the diffraction lines of Pv and Fp appearing within the first 10 min of heating (Fig. 1*A*). Pressure in the sample chamber increased from approximately 130 GPa to approximately 139 GPa over 2.2 h of heating, with Pv stable throughout the heating and without the appearance of any diffraction lines from pPv.

A third sample was heated to 2,300 K at 139 GPa, producing Pv + pPv. Pv + pPv persisted through subsequent heating of the sample with some increase in sample pressure over the 1.5 h heating duration (Fig. 1*B*). The sample was then compressed to approximately 150 GPa and heated between 1,750 K and 2,000 K for 1 h, with the mixed phase persisting throughout the heating cycles up to a pressure of 158 GPa. Heating of a fourth sample to 2,000–2,500 K at approximately 145 GPa produced Pv + pPv that remained stable for 1.2 h at high temperature. This sample was decompressed and heated at approximately 2,200 K at 130 GPa for 1 hour, with the Pv + pPv mixture persisting over the duration of the heating. Our fifth sample was heated to 1,750–2,500 K at 165 GPa, producing Pv + pPv that remained stable throughout 2.2 h of heating. We heated a sixth sample to 2,400 K at 170 GPa for 1 h. Postperovskite crystallized within the first 10 min of heating without any diffraction lines from Pv (Fig. 1*C*).

San Carlos Olivine Composition. A pressure-amorphized San Carlos olivine sample was heated to 2,000 K at 128 GPa for 30 min, synthesizing Pv together with Fp. The temperature was increased to 3,000 K for another 30 min with Pv persisting throughout the heating cycle at 133 GPa (Fig. 1*D*). A second sample was laser heated between 2,700 K and 3,000 K at 135 GPa for a total of 2 h, producing a mixture of Pv + pPv at all temperatures (Fig. 1*E*).

Our third sample was compressed to 135 GPa, with pure pPv appearing after 30 min of heating at 2,500 K and 136 GPa. Pure pPv remained after heating the sample for an additional 30 min at 2,700 K and 139 GPa. The sample was then decompressed and heated at 2,500 K and 134 GPa for 30 min with no evidence of pPv → Pv transformation. The sample was further decompressed and heated to approximately 2,500 K at 132 GPa for 1 h, with only pPv present over the heating duration. Back-transformation inferred by the appearance of Pv lines along with widening and lowering of intensity of pPv lines occurred after a third decompression and heating to approximately 2,000 K at 117 GPa for 50 min.

The fourth sample was laser heated at approximately 3,000 K and 140 GPa for 1 h. pPv was stabilized after 10 min of heating and persisted through the duration of the heating. The sample was then decompressed to 123 GPa, where an unheated sample spot was located and heated at 2,700 K for 10 min, forming pure Pv together with Fp, suggesting the stability of Pv. The sample was then heated in the original spot (used to synthesize pure pPv) at approximately 2,500 K at 126 GPa for a total of 2 h, with a mixed Pv + pPv phase appearing after the first hour of heating. This persistence of Pv + pPv at this pressure–temperature condition is likely due to kinetics because synthesis directly from the glass starting material heated at similar pressure–temperature conditions produced pure Pv.

MORB Composition. In a MORB sample heated at 105 GPa and 3,000 K, we found Pv forms together with other phases in 30 min, indicating this pressure–temperature range corresponds to the stability field of pure Pv (Fig. 1*G*). Another 30 min of heating at these pressure–temperature conditions confirmed the stability of Pv. Pressure was then increased on this sample to 114 GPa and heated to 2,800 K, where diffractions peaks for the pPv phase grew after 30 min and coexisted with Pv, indicating a crossing of the Pv → Pv + pPv boundary. A second sample was taken to 100 GPa and 2,500 K, and again Pv was found to be the stable phase, with no evidence for pPv over 90 min of heating. Pressure was then increased to 105 GPa and 2,800 K, and the sample was still determined to be in the Pv field after 60 min of heating, confirming the stability of Pv at the pressure–temperature range measured from the first sample.

The third MORB sample was first heated at 115 GPa and 2,600 K, and found to be in the mixed-phase field. The sample was then decompressed to 95 GPa and 2,600 K where Pv diffraction peaks grew and the pPv phase disappeared, indicating the stability of Pv. Separate samples were also first synthesized at 118 GPa and 122 GPa and 3,000 K, producing mixed phases over a total of 120 min and 90 min of heating, respectively (Fig. 1*H*).

In a fresh sample, at 126 GPa and 2,500 K, pure pPv was synthesized after 10 min of heating and then remained stable throughout a total of 90 min of heating (Fig. 1*I*). After decreasing pressure slightly, and heating the sample to 2,500–3,000 K, pPv remained the stable phase. Pressure was then further decreased and then heated at 95 GPa and 2,700 K where Pv was found to be stable after 30 min of heating.

Although it is difficult to extract unit cell volume from the α-PbO_2 phase of SiO_2 due to peak overlap, we were able to determine unit cell parameters at 108 and 117 GPa based on 6–8 diffraction peaks. The unit cell parameters at 108 GPa are 3.79(3) Å, 4.71(2) Å, 4.22(4) Å, with a volume of 75.24(5) $Å^3$, and at 117 GPa are 3.76(3) Å, 4.71(4) Å, 4.20(3) Å with a volume of 74.36(6) $Å^3$.

Sources of Uncertainty in the Measurements.
Accurate data analysis requires understanding the sources of error and making an effort to reduce them. The diamond-anvil cell is a uniaxial device that can generate large deviatoric stress that must be reduced for phase relation studies for the mantle. In this study, we use Ar or Ne as a pressure transmitting medium, which are compressible and chemically inert. Our pressure transmitting media also act as thermal insulation for the sample. We observed intense diffraction peaks from the media in all experiments, indicating sufficient insulation separating the sample from the diamond anvils (Fig. 1). This is important because diamond is an excellent heat conductor, resulting in large thermal gradients in the sample if it is not properly insulated. To further reduce the thermal gradients along the radial directions, we made the size of the sample platelet comparable to the size of laser beam focus, as we also did in our binary and ternary study (5). We are not able to quantify the amount of Soret diffusion in our samples because they are loaded with noble gas and are difficult to recover upon decompression. Results from previous studies using solid pressure media indicate some chemical segregation, especially towards the edges of the sample (6, 7). However, the effect has not been quantified using argon pressure media, which may be a good thermal insulator and is chemically inert.

In this study we crossed the boundary along both forward and reverse directions, similar to our previous study (5). This is particularly important to estimate the effects of kinetics on the determined boundary thickness and depth. As shown in Fig. 2, a few data points measured from a previously synthesized Pv + pPv mixture persisted even at the pressure-temperature conditions where pure Pv should be stable according to the data points obtained from fresh starting materials, such as a data point in the pyrolitic composition at 130 GPa and 2,200 K, and a data point in the San Carlos olivine composition at 126 GPa and 2,500 K. The offset in pressure for these data points from the general trend is larger (8 GPa) than our measurements on the binary and ternary systems (5), indicating that the kinetic effects are larger in the multiphase systems presented here. Although kinetics of the Pv → pPv transition and partitioning of elements between Pv and pPv are the main sources of uncertainty in the binary and ternary systems, kinetics of element partitioning among Pv, pPv, and the other coexisting phases that do not participate in the phase transition (such as Fp, silica, and calcium ferrite-type phase) is an important additional source in multiphase systems.

In MORB, because of the relatively small proportion of Mg-silicate (approximately 35 mol%) and its weak scattering, it can be difficult to distinguish between samples that are in the mixed-phase region but near the phase boundary where the fraction of one phase relative to the other may be very high from those in the pure field. This contributes to the error in the location of the boundaries particularly in MORB.

Consideration of the uncertainties in pressure scales is important for comparison among different experimental results and with seismic observations. Although much effort has been made (8), significant uncertainties still exist in the thermal equations of state of pressure standard materials at pressures over 100 GPa. The majority of data points, including both the previous work of other researchers and our studies in Fig. 2, are based on the gold pressure scale. Ohta et al. (9) used a gold scale calibrated to MgO (10) that estimates pressure about 5 GPa higher than the pressure scale (11) used in our study. However, the existing data are not sufficient to validate the accuracy as an absolute pressure scale (12). Considering the discrepancy among recent studies on the gold scale (11, 12), it is reasonable to assume that the gold scale has an uncertainty of about 5 GPa (100 km) at pressures greater than 100 GPa and 2,000 K.

We note that using these same techniques, we have so far investigated a total of six different systems for the depth and thickness of the Pv → pPv transition, together with Catalli et al. (5). Our methods have identified sharp boundaries (0–100 km) in two different systems (San Carlos olivine and $MgSiO_3$-Fe_2O_3), a narrow boundary (100–300 km) in MORB, and broad boundaries in three different systems (pyrolite, $MgSiO_3$-$FeSiO_3$, and $MgSiO_3$-Al_2O_3-Fe_2O_3), demonstrating that the method is capable of measuring a wide range of thicknesses.

Unidentified Diffraction Lines.
A few diffraction peaks in Fig. 1 were not attributable to any of the expected phases. In pyrolite, one diffraction line at approximately 0.6 $Å^{-1}$ appears in the pure Pv diffraction pattern (Fig. 1*A*). The unidentified peak is in all the diffraction patterns of Pv but consists of only a few spots instead of a complete ring.

Three unidentified peaks appear in mixed-phase diffraction patterns in the San Carlos olivine composition (Fig. 1*E*) at approximately 0.62 $Å^{-1}$, approximately 0.67 $Å^{-1}$, and approximately 0.73 $Å^{-1}$. The diffraction line at 0.67 $Å^{-1}$ is spotty and not in all diffraction patterns, and the line at 0.73 $Å^{-1}$ is also spotty as well. The unidentified lines are unique to the San Carlos olivine sample and do not occur in other samples. It is possible that these peaks are from some impurity phases in our natural San Carlos olivine starting material. The observation of the stishovite line in one of San Carlos olivine composition may be due to quartz impurity in the natural sample. One unidentified peak appears in the pure pPv diffraction patterns (Fig. 1*F*) at approximately 0.63 $Å^{-1}$ in San Carlos olivine. This line does occasionally appear in some mixed-phase diffraction patterns in pyrolite and in pure pPv diffraction patterns in MORB. The unidentified peaks in diffraction patterns with pPv could potentially be from structural polymorphism as described in refs. 13 and 14.

In the MORB diffraction patterns, an unknown line appears near approximately 0.36 $Å^{-1}$, at slightly higher *d*-spacing than the 110 line of the $CaCl_2$ phase of silica (Figs. 1 *G* and *I*). This line consistently shows up in the diffraction patterns, independent of the phase diagram of Pv and pPv, but always in the presence of the $CaCl_2$ phase. The morphology of the line in the 2D diffraction image as well as it only being present with $CaCl_2$, suggests that it is likely associated with the silica phase.

Clapeyron Slope of the Pv → pPv Boundary.
The Pv – Pv + pPv boundary in the pyrolitic composition has enough data coverage to estimate a Clapeyron slope of 5.6 ± 0.8 MPa/K, consistent with estimates (6.7 ± 0.5 MPa/K) in ref. 5. Therefore, the Clapeyron slope from ref. 5 is used for the boundaries in Fig. 2.

Effects of Al.
A computation by Tsuchiya and Tsuchiya (15) proposed that Al decreases the depth of the Pv → pPv transition and does not increase the thickness (Fig. 3*B*). However, this study assumed different structural effects of Al from other computational studies, which remains to be investigated by experiments.

Effects of Fe^{3+}.
Our measurements on the Pv – pPv boundary in $MgSiO_3$-Al_2O_3-Fe_2O_3 ternary system give a shallower boundary than other studies on Al-bearing systems (5). However, this is likely due to Fe_2O_3, which decreases the depth and thickness of the

Pv – pPv boundary according to our results on the $MgSiO_3$-Fe_2O_3 binary system (5).

Discrepancy with Previous Studies on Pyrolite.
Previous studies on a pyrolitic composition (3, 9) reported a much shallower and thinner Pv – pPv boundary. A slightly shallower and thinner boundary is expected because they used KLB-1 peridotite composition with about 1 wt% less Al_2O_3 than this study. However, the discrepancy cannot be entirely attributable to the slight compositional differences. They used a different gold scale (16), but this scale should affect the depth (increase by 5 GPa), but not the thickness. They used two different sample setups: sample platelet coated with 60 nm thick gold coatings and platelets of the sample+gold powder mixture. They used NaCl as a medium, which may be more rigid and reactive than noble gas medium. Because of the solubility of Na in Pv and pPv, if Na can be supplied to the system, it could affect the stability of these phases in pyrolite, whereas it is less likely the case for MORB because this composition already has a high Na content. For the starting material, they used a gel, whereas we used an anhydrous glass material. Their dataset also includes data points with a few minutes of short heating duration.

A more recent study on a pyrolitic composition (17) reported pure pPv after heating to approximately 2,400 K at 135 GPa. However, the pressure was measured after laser heating. This study used silica as a pressure transmitting medium, which may support larger deviatoric stresses and elevate silica activity in the system. Therefore, it is difficult to compare with our results.

1. Tangeman JA, Phillips BL, Navrotsky A, Weber JKR, Hixson AD, Key TS (2001) Vitreous forsterite (Mg_2SiO_4): Synthesis, structure, and thermochemistry. *Geophys Res Lett* 28:2517–2520.
2. McDonough WF, Sun SS (1995) The composition of the earth. *Chem Geol* 120:223–253.
3. Murakami M, Hirose K, Sata N, Ohishi Y (2005) Post-perovskite phase transition and mineral chemistry in the pyrolitic lowermost mantle. *Geophys Res Lett* 32:L03304.
4. Presnall DC, Hoover JD (1987) in *Magmatic Processes: Physiochemical Principles*, ed Mysen B (Geochemical Society, St. Louis, MO), Vol 1, pp 75–80.
5. Catalli K, Shim SH, Prakapenka V (2009) Thickness and Clapeyron slope of the post-perovskite transition. *Nature* 462:782–785.
6. Heinz D, Jeanloz R (1987) Measurement of the melting curve of $Mg_{0.9}Fe_{0.1}SiO_3$ at lower mantle conditions and its geophysical implications. *J Geophys Res—Solid* 92:11437–11444.
7. Sinmyo R, Hirose K (2010) The Soret diusion in laser-heated diamond-anvil cell. *Phys Earth Planet Inter* 180:172–178.
8. Fei Y, Ricolleau A, Frank M, Mibe K, Shen G, Prakapenka V (2007) Toward an internally consistent pressure scale. *Proc Natl Acad Sci USA* 104:9182–9186.
9. Ohta K, Hirose K, Lay T, Sata N, Ohishi Y (2008) Phase transitions in pyrolite and MORB at lowermost mantle conditions: Implications for a MORB-rich pile above the core-mantle boundary. *Earth Planet Sc Lett* 267:107–117.
10. Speziale S, Zha CS, Duy TS, Hemley RJ, Mao HK (2001) Quasi-hydrostatic compression of magnesium oxide to 52 GPa: Implications for the pressure-volume-temperature equations of state. *J Geophys Res* 106:515–528.
11. Tsuchiya T, Tsuchiya J, Umemoto K, Wentzcovitch RM (2004) Phase transition in $MgSiO_3$ perovskite in the Earth's lower mantle. *Earth Planet Sc Lett* 224:241–248.
12. Hirose K, Sata N, Komabayashi T, Ohishi Y (2008) Simultaneous volume measurements of Au and MgO to 140 GPa and thermal equation of state of Au based on the MgO pressure scale. *Phys Earth Planet Inter* 167:149–154.
13. Oganov AR, Ono S (2005) The high-pressure phase of alumina and implications for Earth's D″ layer. *Proc Natl Acad Sci USA* 102:10828–10831.
14. Tschauner O, Kiefer B, Liu H, Sinogeikin S, Somayazulu M, Luo SN (2008) Possible structural polymorphism in Al-bearing magnesiumsilicate post-perovskite. *Am Mineral* 93:533–539.
15. Tsuchiya J, Tsuchiya T (2008) Postperovskite phase equilibria in the $MgSiO_3$-Al_2O_3 system. *Proc Natl Acad Sci USA* 105:19160–19164.
16. Hirose K, Sinmyo R, Sata N, Ohishi Y (2006) Determination of post-perovskite phase transition boundary in $MgSiO_3$ using Au and MgO pressure standards. *Geophys Res Lett* 33:L01310.
17. Sinmyo R, Hirose K, Muto S, Ohishi Y, Yasuhara A (2011) The valence state and partitioning of iron in the Earth's lowermost mantle. *J Geophys Res* 116:B07205.

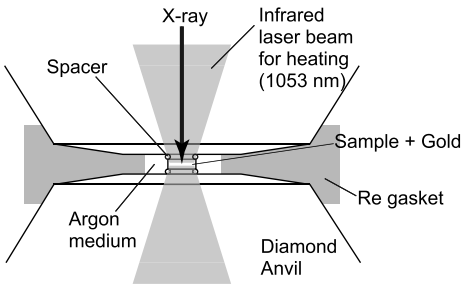

Fig. S1. Schematic diagram of the sample setup in laser-heated diamond-anvil cell.

Table S1. Chemical compositions of glass starting materials for Ca-free pyrolite and MORB (in oxide wt%)

	Pyrolite	MORB
SiO_2	45.6	49.6
Al_2O_3	4.9	16.6
FeO	8.7	7.9
MgO	40.8	9.7
CaO	-	13.4
Na_2O	-	2.8